Aalborg Universitet

Waste incineration and heat recovery hybridized with low-focus fresnel lens solar collectors for sustainable multi-generation

A thorough techno-economic-environmental analysis and optimization

Wang, Lina; Teles, Mavd P.R.; Yu, Haoshui; Silva, Brenda V.F.; Arabkoohsar, Ahmad

Published in:
Chemosphere

DOI (link to publication from Publisher):
10.1016/j.chemosphere.2023.140409

Creative Commons License
CC BY 4.0

Publication date:
2024

Document Version
Publisher's PDF, also known as Version of record

Link to publication from Aalborg University

Citation for published version (APA):
Wang, L., Teles, M. P. R., Yu, H., Silva, B. V. F., & Arabkoohsar, A. (2024). Waste incineration and heat recovery hybridized with low-focus fresnel lens solar collectors for sustainable multi-generation: A thorough techno-economic-environmental analysis and optimization. *Chemosphere*, *346*, Article 140409. https://doi.org/10.1016/j.chemosphere.2023.140409

General rights
Copyright and moral rights for the publications made accessible in the public portal are retained by the authors and/or other copyright owners and it is a condition of accessing publications that users recognise and abide by the legal requirements associated with these rights.

- Users may download and print one copy of any publication from the public portal for the purpose of private study or research.
- You may not further distribute the material or use it for any profit-making activity or commercial gain
- You may freely distribute the URL identifying the publication in the public portal -

Take down policy
If you believe that this document breaches copyright please contact us at vbn@aub.aau.dk providing details, and we will remove access to the work immediately and investigate your claim.

Downloaded from vbn.aau.dk on: July 04, 2025

Chemosphere 346 (2024) 140409

Contents lists available at ScienceDirect

Chemosphere

journal homepage: www.elsevier.com/locate/chemosphere

Waste incineration and heat recovery hybridized with low-focus fresnel lens solar collectors for sustainable multi-generation; A thorough techno-economic-environmental analysis and optimization

Lina Wang [a,b], Mavd P.R. Teles [b], Haoshui Yu [c], Brenda V.F. Silva [b], Ahmad Arabkoohsar [d,*]

[a] *School of Marine Technology and Environment, Dalian Ocean University, Dalian, China*
[b] *Energy Department, Aalborg University, Denmark*
[c] *Department of Chemistry and Bioscience, Aalborg University, Denmark*
[d] *Department of Civil and Mechanical Engineering, Technical University of Denmark, Kgs. Lyngby, Denmark*

HIGHLIGHTS

- Waste incineration and waste heat recovery support solar energy for sustainable multigeneration.
- 100% clean and stable low-grade heat, power, and industrial heat are produced year-round.
- Fresnel lens thermal collectors with cheap micro-structured foils are used to reduce investment costs.
- A benchmarking analysis is conducted to show the importance of industrial heat supply.
- The levelized cost of energy (LCOE) is 23.96 €/MWh.

GRAPHICAL ABSTRACT

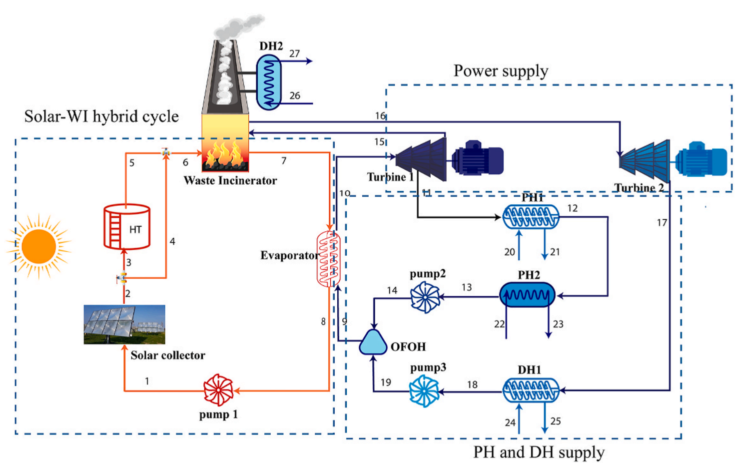

ARTICLE INFO

Handling Editor: Pouria Ahmadi

Keywords:
Waste incineration
Fresnel lens solar collector
Stable renewable production
Multi-objective programming
Hybrid tri-generating power plant

ABSTRACT

Biomass, including municipal solid waste, and solar energy are two of the inevitable sources for future decarbonized energy systems. Fresnel lens thermal collectors using cheap micro-structured foils is an interesting emerging medium-temperature solar thermal design that might be of high practical value, provided that its fluctuating output is managed. This study proposes a hybrid solar-waste solution using this type of collector for multi-generation via an Organic Rankine Cycle. The cycle is specially designed for supplying low-grade heat, power, and industrial heat (which is a very critical sector to be decarbonized) taking advantage of the generated stable solar-waste medium-temperature heat at zero emission level. To achieve this optimal design, the article conducts a thorough energy-exergy-economic-environment (4E) analysis of the system and employs the non-dominated sorting genetic algorithm (NSGA II) for the optimizations. A benchmarking analysis is also

* Corresponding author.
E-mail address: ahmar@dtu.dk (A. Arabkoohsar).

https://doi.org/10.1016/j.chemosphere.2023.140409
Received 22 May 2023; Received in revised form 20 September 2023; Accepted 9 October 2023
Available online 11 October 2023
0045-6535/© 2023 The Authors. Published by Elsevier Ltd. This is an open access article under the CC BY license (http://creativecommons.org/licenses/by/4.0/).

conducted to show the importance of industrial heat supply in this cycle. The results show that this hybridization, owing to the cheap and flexible heat delivery of the waste incinerator as well as the low cost of the solar collectors, is very effective for efficient and cheap multi-generation. Especially for industrial heat supply, the competitive levelized cost of energy (LCOE) of 23.96 €/MWh is obtained, which is way lower than today's achievable costs in the industry.

1. Introduction

Due to the rapid development of industrialization and growing population, energy demand is also overgrowing. Approximately 70% of the world's energy demands are met by fossil fuels (Aghaziarati and Aghdam, 2021). The consumption of fossil fuels causes environmental problems, such as carbon dioxide emissions. The report on the global energy outlook predicts that by 2040, the world's energy demand will increase 20–30% (Newell et al., 2019). The sustainability of energy systems stands on several critical pillars. These are renewable energy, maximum utilization of available resources including waste sources, energy storage, decarbonization of different sectors via e.g., electrification, etc. (Kalbasi et al., 2023).

According to the Renewable Energy Agency, by 2050 renewable energy sources must provide at least 90% of the energy required for combined space heating and power generation to achieve the "1.5 °C″ global warming limitation objective (Rogelj et al., 2019; Gao et al., 2022). Reducing environmental pollution, notably greenhouse gas emissions, is the main advantage of using renewable energy sources (Shahsavari and Akbari, 2018). Solar technologies could come in a variety of classes for various sectors, including thermal solutions for heat supply at low and medium temperatures, for high-temperature heat supply so that power could be used via conventional power block designs, direct power generation via PV systems, or hybrid solutions such as PVT systems (Ravi Kumar et al., 2021). Usually, the conversion efficiency of solar thermal systems is higher than solar PV systems (Kumar et al., 2019). The most popular heat solar conversion system technique is concentrated solar power (CSP), which uses costly glass mirrors and receivers. The most common four CSP technologies so far have been heliostats, parabolic dishes, linear Fresnel reflectors, and parabolic trough collectors (PTC), all of which are yet more expensive than conventional competing methods of energy supply (Desai et al., 2021). However, there is a novel Fresnel lens thermal collector based on micro-structured polymer foil, which is much more promising in terms of costs, although it does not provide too high temperatures and lies in the class of medium-temperature solar solutions (Pranov et al., 2019). According to Desai et al. (2022), compared to PTC-based plants, the Fresnel lens thermal collectors power plant can lower the levelized cost by as much as 40%. Apart from this, despite the huge potential in this class of solar technology, there is not much more research and assessments about this collector in the literature, being an inspiration for the current research study.

On the other hand, regardless of specific technology, one of the biggest challenges with solar systems is the intermittency of output energy (Gowrisankaran et al., 2016). There are two effective solutions to this challenge. One is the energy storage technique, and the other is hybridization with stable and agile heat sources (Jie Ling et al., 2022; Ortiz et al., 2021). For solar thermal, which is the focus of this work, if combined with an energy storage unit, although thermal storage is not too costly per MWh for instance, securing continuous energy supply is yet very expensive. This is mainly due to two major reasons: 1) the huge required volume due to the night hours as well as several daily occasions that solar energy is not sufficiently available, and 2) the oversized solar field to enable sufficient overproduction during sunny hours for off-sun times. Therefore, hybridization provided that a sustainable, agile, and cheap source of stable energy is available can be a very effective measure. One of these supplementary sources is waste incineration (WI) which has been economical and environmentally friendly as well (Escamilla-García et al., 2020). Indeed, the two primary methods used for treating and disposing of municipal solid waste (MSW) are landfilling and incineration (Jack and Oko, 2017), among which WI has turned out to be a more effective way of reducing the toxicity and volume of MSW; it also can prevent soil and water contamination (He and Lin, 2019). WI is more used in Europe, notably in Germany and Denmark. Hybrid solar-WI systems in various configurations have also been studied in the past and promising results such as output stability, increased effectiveness, and lower capital expenditures due to equipment sharing have been obtained. Sadi and Arabkoohsar (2019a) proposed a cost-effective and dispatchable electricity solar-WI system, in which the net annual energy efficiency is about 24%.

When solar heat is supplied, there must be a power block to convert this to power or provide multi-vector energies. As the low-focus Fresnel lens solar collector of this work cannot generate too high temperatures, conventional power cycles such as Rankine and Brayton could not be the optimal solutions for integration. Indeed, an ORC system is usually used for effective electricity production when the temperature is no more than 400 °C (Naquash et al., 2023; Gomaa et al., 2020). One of the most crucial advantages of the ORC system is that it can be applied on minor scales. In addition to solar energy, other renewable energy sources (such as biomass and industrial waste heat) can be coupled to the ORC system (Yu et al., 2023; Liu et al., 2023). Bellos et al. (Bellos and Tzivanidis, 2018) suggest a hybrid system driven by solar energy and waste heat, which investigates the effect of working fluids and the output power of the system. The results concluded that the best fluid option is toluene, which has a system efficiency range of 11.6%–19.7%. Chen et al. (2022) established a waste heat recovery combined with a solar ORC system and concluded that solar energy can increase efficiency and reduce the distillation system's overall annual cost. The multi-objective optimization (NSGA-II) approach was used to conduct optimization research on the WI combined ORC system, focusing on reducing energy use and enhancing economic and environmental performance. Jafary et al. (2021) performed an ORC system in which an internal heat exchanger (IHE) was implemented (ORC-IHE). Compared to regeneration ORC, the overall energy efficiency and exergy efficiency of the ORC-IHE-based system are higher for the whole system driven by PTC. Behzadi et al. (2021) analyzed hybrid MSW-solar power plants that substantially affect production costs and emissions.

Another important point here is that although sustainable energy supply in several sectors is being addressed at an effective pace, it has been a challenge to decarbonize the industrial heating sector. Nearly 70% of process heat demand is supplied by fossil fuels which are mainly available in conflicted regions. To minimize such dependency, the EU developed the REPowerEU plan targeting cost-effective, reliable, and sustainable energy solutions (Serda et al., 2022). Process heating (PH) systems typically use a device that generates heat and a heat transfer mechanism for transporting that from the production site to the process site (Crespo et al., 2019). PH at high temperatures is largely needed in many industries including agriculture, textiles, food, tobacco, electrical apparatus, clothing, leather, paper, chemicals, metals, etc. Most of which fossil fuels have been the dominating source (Farjana et al., 2018). Solar heat at any temperature within the range of temperatures needed in the industry could be of high practical value to bring sustainability to this sector as well (Aboelwafa et al., 2018). The literature provides several examples of such applications. Jinshah et al. (2023), for instance, focus on an open natural circulation loop-based PTC for process heat at low temperatures, which aims to enhance efficiency and reduce the levelized cost of heat and payback time. Amen et al. (2021) collected some samples of MSW from Lahore, and the sample's higher heating values (HHV) were thoroughly quantified. The hybrid energy system of geothermal and wind energy resources is also proposed to produce hydrogen chloride, the payback time is 2.7 years, and the additive value of hydrogen chloride is 0.0642 $/kg (Mehrpooya et al., 2021). There are also other articles focused on hybrid energy systems, such as solar-biomass cooling cogeneration systems (Morais et al., 2020; Meriño Stand et al., 2021) and solar-combined geothermal power generation systems (Song et al., 2021).

As mentioned before, despite several pieces of research on conventional CSP or PTC for a variety of purposes, including PH, very few studies could be found on Fresnel lens collectors and their combination with any other supplementary sources. Understanding the gap, having a solid knowledge foundation of solar and hybrid systems for multi-generation, and the importance of the sectors thirsty for sustainability, this article proposes an innovative hybrid solar-WI tri-generating ORC system for maximum technical, sustainability, and economic benefits. The results of this 4E analysis and multi-objective optimizations on the proposed system for a case study in China are compared with those of a similar hybrid system that does not offer PH. The confluence of several key factors, including a readily available supply of PH, the decreased cost of solar collectors, and the implementation of multi-objective optimizations, synergistically enhances the overall economic viability of the system while concurrently mitigating carbon emissions. The followings are the facts making this article innovative.

- The innovative hybrid design for medium temperature solar-waste driven ORC, using its specific solar collector and hybridized by WI for stable supply.
- Sustainable PH supply parallel with district heating and electricity supply via a renewable-based low-grade power system.
- NSGA-II Multi-objective optimization with a complex algorithm for achieving optimal design and operating setpoints, thereby improving the system's economic, environmental, and energetic impacts.
- Using TOPSIS (Technique for Order Preference by Similarity to Ideal Situation) to find the optimum operation of the system where the optimization functions contradict each other as the decision variables change.

2. Proposed system

The system consists of two interconnected subsystems: the solar cycle and the ORC. The extracted output from the first turbine is directed back to the incinerator for the purpose of reheating. Fig. 1 depicts the schematic of the proposed hybrid system. As seen, solar energy is collected by the solar collectors and is stored in a storage tank (HT), if needed. Then, the liquid will be reheated in the WI before going through the evaporator. After exchanging heat with the ORC medium in the evaporator, the working fluid (WF) comes back to the solar collectors. Therminol 66 is chosen as the WF.

The ORC, naturally, contains four main parts, namely, the evaporator, the turbines, condenser, and pump. Toluene is the WF in this cycle due to its high efficiency after optimization compared to other candidate fluids for this temperature level (Yu et al., 2021). A certain amount of steam is extracted from the first turbine to supply PH to the industry. The rate of extraction has a direct impact on the amount of deliverable low-grade heat (for district heating, DH) and power. After extracting the WF goes through two heat exchangers. Considering the possibilities of PH end-users in real-life applications, two different scenarios are considered here. These are (i) a high-temperature PH network with supply and return temperatures of 160 and 30 °C; (ii) a medium-temperature PH network with collection and return temperatures of 90 and 30 °C. The WF coming out of the heat exchangers considered for the PH are to be pumped to the pressure level required at the evaporator inlet, then the two WFs are mixed in an open feed-organic heater (OFOH). The extraction of the first turbine is defined as α (which is $\dot{m}_{11}/\dot{m}_{10}$). The rest of the WF is re-heated and prepared for the second turbine inlet. The summation of the rotational work produced by the two turbines is used for electricity generation. The third and fourth heat generation parts of the cycle are for supporting a

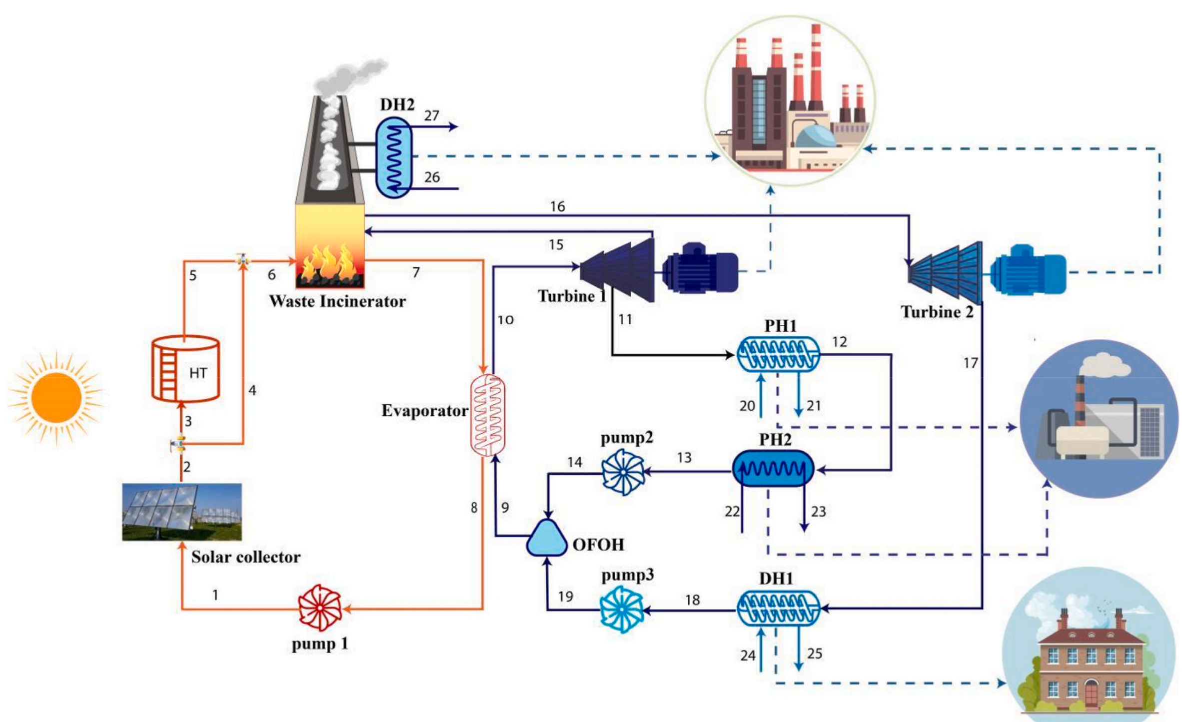

Fig. 1. Schematic of the proposed solar-WI tri-generating system.

low-temperature DH network with supply and return temperatures of 60 and 30 °C, supplied by the main condenser of the ORC as well as the flue gas condensation unit of the WI. Regarding the latter, the flue gas condensation unit, since one of the main reasons for the energy losses is the high energy content of the exhaust of the WI unit, so far simply being wasted to the ambient in many plants (Olabi et al., 2021), this unit is considered to recover a big amount of energy via sensible heat exchange (temperature lowering of the gas) and condensation of the water content of the gas (to reach the higher heating value of the fuel). This will improve the efficiency of the whole cycle and considerably reduce pollutant emissions.

The design parameters of the system are listed in Table 1, and to make the formulation more manageable, the following logical presumptions are used.

- It is assumed that solar radiation is constant during every hour.
- During the process, pressure drop and mass loss were not considered.
- The waste utilized in the WI unit is evenly distributed and provides the same calorific value.
- The impacts of system component activity outside of specifications are disregarded.
- Each turbine and pump have an isentropic efficiency of 0.85.

3. Methodology

3.1. Energy and exergy analysis

The heat transfer rate $\dot{Q}_{SC}$ of Fresnel lens thermal collectors can be calculated as (Desai et al., 2021):

$$\dot{Q}_{SC} = \left(\eta_o \cdot DNI \cdot IAM \cdot be \bullet bsh - U_{SC} \bullet \left(T_{SC,m} - T_0 - \dot{Q}_{pipe}\right)\right) \bullet A_{ap} \tag{1}$$

$$\dot{Q}_{SC} = \dot{m}_{SC} \bullet \left(h_{SC,out} - h_{SC,in}\right) \tag{2}$$

The parameter of the whole system is calculated by the routine testing procedure offered by a company in Denmark. Where η_o is the optical efficiency of the solar collector, DNI is the direct normal irradiance, IAM is the incidence angle modifier, and *be* and *bsh* are the end-losses and shadow-losses of the solar collector, which is related to the design of the collector, and it is overlooked in this investigation. U_{SC} is the heat-loss coefficient of the collector. $T_{SC,m}$ is the average temperature of the collector, T_0 is the ambient temperature, $\dot{Q}_{pipe}$ is the loss of heat and pressure through the pipes, which is related to the design, and it is also neglected. A_{ap} is the aperture area of the solar collector, each collector lens measures 153cm × 140 cm, and each receiver is 25cm × 25 cm. One solar collector device contains eight lenses and eight receivers.

Table 1
Design parameters for the hybrid system (Nami et al., 2019).

Parameters	Symbol	Value
The lower heating value of the waste (kJ/kg)	LHV	12,500
Waste compositions (weight percent %)	Ash	5.91
	Carbon	47.18
	Hydrogen	6.25
	Oxygen	39.57
	Nitrogen	0.91
	Sulphur	0.18
Tape of waste	Municipal solid waste	
Flu gas temperature of the stack before (°C)	T_in	165
Flu gas temperature of the stack after (°C)	T_out	45
Outlet temperature of the collector (°C)	T_2	280
The inlet temperature of the first turbine (°C)	T_{10}	245
The optical efficiency of solar collector	η_o	0.833
heat-loss coefficient of solar collector	U_{SC}	0.85
The temperature of the sun (°C)	T_sun	5800
The efficiency of waste heat	η_{WI}	0.8
Room temperature (°C)	T_0	25
Atmospheric pressure (kPa)	P_0	101.325

The number of solar collector units in a series and the number of rows is based on the temperature required. $\dot{m}_{SC}$ is the mass flow rate of the solar field, $h_{SC,out}$ and $h_{SC,in}$ is the enthalpy of outlet and inlet WF through the solar collector.

For the WI unit, the effective way to calculate the energy level released in the WI unit is using an average lower heating value (LHV) of the waste source. If the waste is evenly distributed, the reported LHV is around 12,500 kJ/kg (Arabkoohsar and Nami, 2019). The thermal power of this process $\dot{Q}_{WI}$ can be described as:

$$\dot{Q}_{WI} = \eta_{WI} \bullet \dot{m}_{WI} \bullet LHV \tag{3}$$

where, η_{WI} is the efficiency of the incineration process, which is usually around 70%–80%. In the present work, it is assumed to be 80%. And $\dot{m}_{WI}$ is the mass flow rate of the waste.

The mass balance of the flue gas is (Coskun et al., 2009):

$$m_{WI} + m_{air} = m_{flue\ gas} + m_{ash} \tag{4}$$

The equation below can be used to calculate the necessary air volume. It depends on the fuel's chemical component and the extra air ratio (Coskun et al., 2009).

$$m_{air} = (2.9978 \times K_H - 0.3747 \times K_O + 0.3747 \times K_S + K_C) \times (11.445 \times n) \tag{5}$$

where K_H, K_O, K_S, and K_C stand for the element's percentage in the chemical composition (%) (Coskun et al., 2009).

$$n = 1 + \lambda \tag{6}$$

λ is the percentage of extra combustion air, when n equal to 1 (in our work $n = 1$), the stoichiometric air amount is (Coskun et al., 2009):

$$m_{air} = (2.9978 \times K_H - 0.3747 \times K_O + 0.3747 \times K_S + K_C) \times (11.445) \tag{7}$$

The m_{air} means the air demand of the fuel per kilogram. Then the flue gas can be expressed as (Coskun et al., 2009):

$$m_{flue\ gas} = (2.9978 \times K_H - 0.3747 \times K_O + 0.3747 \times K_S + K_C)s \times (11.445 \times n) + m_{WI} - m_{ash} \tag{8}$$

during the burning process, the flue gas temperature range is $100 \sim 1200°C$.

Exergy reflects the thermodynamic properties of the system. Generally, there are four components of exergy: potential exergy, chemical exergy, physical exergy, and kinetic exergy. This work considers physical and chemical exergy. The physical exergy at each state point can be stated as (Teng et al., 2021):

$$\dot{\varepsilon}_i = \dot{m}[(h_i - h_0) - T_0(s_i - s_0)] \tag{9}$$

where h_0 and s_0 are the enthalpy and entropy of the working fluid at standard atmospheric pressure and room temperature. The exergy balance equation of each unit can be written as:

$$\sum \dot{\varepsilon}_{in} = \sum \dot{\varepsilon}_{out} + \dot{I} \tag{10}$$

where $\sum \dot{\varepsilon}_{in}$ and $\sum \dot{\varepsilon}_{out}$ are the exergy flowing in and out per unit, and $\dot{I}$ is the exergy destruction. The chemical exergy is mainly about the MSW. When the elemental composition is known, it is possible to compute the fuel exergy of MSW using an empirical correlation proposed by (Sajid Khan et al., 2022):

$$\dot{\varepsilon}_x = LHV \times \dot{m}_{WI}\left(1.0064 + \frac{0.1519H}{C} + \frac{0.0616O}{C} + \frac{0.0429N}{C}\right) \tag{11}$$

where H, C, N, and O stand for, respectively, the concentrations of hydrogen, carbon, nitrogen, and oxygen in MSW.

There are two essential parameters to describe the efficiency of the system. One is energy efficiency η_E and the other one is exergy efficiency η_ε, which are defined as:

$$\eta_E = \frac{\left(\sum \dot{Q}_{PHs\ and\ DHs} + \dot{W}_{net}\right)}{\dot{Q}_{supply}} \tag{12}$$

$$\eta_\varepsilon = \frac{\left(\dot{\varepsilon}_{all} - \sum \dot{I}\right)}{\dot{\varepsilon}_{all}} \tag{13}$$

where $\dot{W}_{net}$ is the total power output of the ORC system. $\sum \dot{Q}_{PHs\ and\ DHs}$ is the total heat delivered by the system to the PHs and DHs. $\dot{Q}_{supply}$ is the heat input that drives the system. $\dot{\varepsilon}_{all}$ is all the available exergies. And $\sum \dot{I}$ is the total exergy destruction of the whole system. The energy and exergy balance of each component are shown in Table 2.

3.2. Pinch temperature

During the heat exchange process in the evaporator, there are single-phase and two-phase regions. If the viscous dissipation and heat loss are neglected, the energy balance equations can be expressed as (Li et al., 2012):

$$\dot{m}_9(h_{10} - h_{9a}) = \dot{m}_7 \bullet c_{p7}\left(T_7 - T_{c,p}\right) \tag{14}$$

$$\dot{m}_9(h_{9a} - h_9) = \dot{m}_7 \bullet c_{p7}\left(T_{c,p} - T_8\right) \tag{15}$$

where h_{9a} and h_{10} are the enthalpy of the organic WF under saturated liquid condition and saturated vapor condition, respectively, and c_p is the specific heat of the WF.

$$T_{c,p} = T_{9a} + \Delta T_{eva} \tag{16}$$

ΔT_{eva} is the pinch temperature of the evaporator which means the smallest temperature difference between the two types of WF through the evaporator. During the process in the evaporator, the WF sensible heat to latent heat ratio is defined as:

$$Ja = (h_{9a} - h_9) \Big/ (h_{10} - h_{9a}) = \left(T_{c,p} - T_8\right) \Big/ \left(T_7 - T_{c,p}\right) \tag{17}$$

During the heat exchange process, the absorbed heat can be written as:

$$\dot{Q}_{eva} = \dot{m}_9(h_{10} - h_9) = \dot{m}_7 \bullet c_{p7}\left(T_7 - T_{c,p}\right)(1 + Ja) \tag{18}$$

3.3. Economic analysis

There are numerous strategies for co-generation plant economic optimization. The most popular ones are based on energy economic optimization. The net present value (NPV) method evaluates the system's financial performance. It calculates the profit of the system and gives the payback time based on the output energy of system. A system NPV can be determined by using the formula (Arabkoohsar and Nami, 2019):

$$NPV = \sum_{t=1}^{N} Y_t (1 + r)^{-t} \tag{19}$$

Where t is the system economic lifetime, considered as 25 years in this work. Y_t is the net cash flow at the end of the tth year, r is the interest rate, which is 10%. Y_t can be calculated as:

$$Y_t = C_e + C_h \tag{20}$$

C_e and C_h are the electricity and heat cash flow from selling the electricity and heat. Typically, the net cash flow should be minus the cost of biomass and ash disposal. In our case, they are included in the annual operating expenses.

Electricity selling prices can have different ranges according to each EU state member. It can reach a minimum value of 81.2 €/MWh in Slovakia. Or a maximum of 198 €/MWh in Italy. Most cases vary between 90 and 120 €/MWh. Similar variations in DH energy selling prices across many nations in central European often vary between 40 and 75 €/MWh (Braimakis et al., 2021). Because of the energy shortage problem in Europe, the electricity and heat prices are higher than before. Therefore, a base-case value of 100 €/MWh for electricity and 60 €/MWh for DH are assumed in the current work. The PH energy selling prices should be higher than DH, then it is assumed as 75 €/MWh.

It is necessary to define the initial investment considering the economy of the whole system. It includes three parts: the cost of each unit, installation, and operating cost. For heat exchangers, such as evaporators and condensers, the price of each department related to the heat transfer area can be calculated as (Teng et al., 2021):

$$A_i = \frac{\dot{Q}_i}{U_i \Delta T_m} \tag{21}$$

Where U_i is the heat transfer coefficient, and ΔT_m is the expression for the logarithmic mean temperature difference between the fluid on the two sides of the heat exchanger:

$$\Delta T_m = \frac{(\Delta T_{max} - \Delta T_{min})}{\ln\left(\Delta T_{max} / \Delta T_{min}\right)} \tag{22}$$

The capital investment cost of each component is shown in Table 3. The investment is expressed as:

$$Z_{inv} = Z_{WI} + Z_{SC} + Z_{HT} + Z_{T1} + Z_{T2} + Z_{p2} + Z_{p3} + Z_{eva} + Z_{PH1} + Z_{PH2} + Z_{DH1} + Z_{DH2} \tag{23}$$

Table 2
Energy and exergy balance equation of the system.

Component	Energy balance equations	Exergy destruction equations
Collector	$\dot{Q}_{SC} = \dot{m}_{SC}(h_2 - h_1)$	$\dot{I}_{SC} = \dot{e}_1 - \dot{e}_2 + A_{ap} \bullet N \bullet DNI \bullet L_{SC}$ $L_{SC} = 1 - 4T_0/3T_{sun} + 1/3(T_0/T_{sun})^4$
WI	$\dot{Q}_{WI} = \dot{m}_7(h_7 - h_6) + \dot{m}_{16}(h_{16} - h_{15}) + \dot{Q}_{WISC}$	$\dot{I}_{WI} = \dot{e}_{WI} + \dot{e}_6 + \dot{e}_{15} - \dot{e}_7 - \dot{e}_{16} + \dot{I}_{WISC}$
Evaporator	$\dot{Q}_{eva} = \dot{m}_9(h_{10} - h_9) = \dot{m}_7(h_7 - h_8)$	$\dot{I}_{eva} = \dot{e}_7 + \dot{e}_9 - \dot{e}_8 - \dot{e}_{10}$
Turbine 1	$\dot{W}_{t1} = \dot{m}_{10}h_{10} - \dot{m}_{11}h_{11} - \dot{m}_{15}h_{15}$	$\dot{I}_{t1} = \dot{e}_{10} - \dot{e}_{11} - \dot{e}_{15} - \dot{W}_{t1}$
Turbine 2	$\dot{W}_{t2} = \dot{m}_{16}h_{16} - \dot{m}_{17}h_{17}$	$\dot{I}_{t2} = \dot{e}_{16} - \dot{e}_{17} - \dot{W}_{t2}$
PH1	$\dot{m}_{11}(h_{11} - h_{12}) = \dot{m}_{21}(h_{21} - h_{20})$	$\dot{I}_{PH1} = \dot{e}_{11} + \dot{e}_{20} - \dot{e}_{12} - \dot{e}_{21}$
PH2	$\dot{m}_{12}(h_{12} - h_{13}) = \dot{m}_{22}(h_{23} - h_{22})$	$\dot{I}_{PH2} = \dot{e}_{12} + \dot{e}_{22} - \dot{e}_{13} - \dot{e}_{23}$
DH1	$\dot{m}_{17}(h_{17} - h_{18}) = \dot{m}_{24}(h_{25} - h_{24})$	$\dot{I}_{DH1} = \dot{e}_{17} + \dot{e}_{24} - \dot{e}_{25} - \dot{e}_{18}$
DH2	$\dot{m}_{26}(h_{27} - h_{26}) = \dot{m}_{flue\ gas}cp_{flue\ gas}(T_{in} - T_{out})$	$\dot{I}_{DH3} = \dot{e}_{26} - \dot{e}_{27} + \dot{I}_{flue\ gas}$
Pump 2	$\dot{W}_{p2} = \dot{m}_{14}(h_{14} - h_{13})$	$\dot{I}_{p2} = \dot{e}_{13} - \dot{e}_{14} + \dot{W}_{p2}$
Pump 3	$\dot{W}_{p3} = \dot{m}_{18}(h_{19} - h_{18})$	$\dot{I}_{p3} = \dot{e}_{18} - \dot{e}_{19} + \dot{W}_{p3}$

Table 3
Cost function for each element.

Component	Cost function
Waste Incinerator	$Z_{WI} = 2567 \bullet (3600 \bullet m_{WI})^{0.67}$ (Sajid Khan et al., 2022)
Solar collector	$Z_{SC} = 250 \bullet A_p \bullet N$ (Desai et al., 2021)
Hot tank	$Z_{HT} = 250 \bullet V_{TES}$ (Sadi et al., 2021)
Turbine 1	$Z_{T1} = 4750 \bullet \dot{W}_{t1}^{0.75}$ (Alirahmi et al., 2021a)
Turbine 2	$Z_{T2} = 4750 \bullet \dot{W}_{t2}^{0.75}$ (Alirahmi et al., 2021a)
Pump 2	$Z_{p2} = 3500 \bullet \dot{W}_{p2}^{0.41}$ (Alirahmi et al., 2021b)
Pump 3	$Z_{p3} = 3500 \bullet \dot{W}_{p3}^{0.41}$ (Alirahmi et al., 2021b)
Evaporator	$Z_{eva} = 276 \bullet A_{eva}^{0.88}$ (Alirahmi et al., 2021b)
PH	$Z_{PH} = 516.62 \bullet A_{PH}^{0.6}$ (Arabkoohsar and Nami, 2019)
DH	$Z_{DH} = 309.14 \bullet A_{DH}^{0.85}$ (Alirahmi et al., 2023)

Depending on the technology, the annual maintenance costs (service, periodic maintenance, and repairs) can be expressed as a percentage of the investment outlay or as a unitary cost of the annual energy output. For this parameter, various references suggest various levels ranging from 1% up to 6%. In the present work, as suggested in Ref. (Fixed and variable costs for, 2021), 3% of the total investment of the system is used for the economic analyses.

$$Z_{ope} = 0.03 Z_{inv} \tag{24}$$

The same was considered for the installation cost:

$$Z_{ins} = 0.2 Z_{inv} \tag{25}$$

Then the total initial investment is:

$$Z_{total} = Z_{ope} + Z_{ins} + Z_{inv} \tag{26}$$

The relationship between total investment Z_{total} and net investment flow Y_t can be measured by payback time. It means that the time value when accumulated with the Y_t goes from a negative value to a positive value.

A helpful summary assessment of the overall competitiveness of various power generation choices is implied by the term Levelized cost of energy (LCOE). It is equivalent to the ratio of the overall cost incurred throughout the course of the project to the amount of electricity the installation will produce during its useful life, and the PH and DH supply. The LCOE considers the associated energy production and total installation expenses incurred over the project (Allouhi et al., 2019). In this way, the LCOE is calculated using the following equation (Petrollese and Cocco, 2019).

$$LCOE = \frac{\left(Z_{inv} + \sum_{i=1}^{N} Z_{ope}/(1+i)^n\right)}{\left(\sum_{i=1}^{N} (\dot{Q}_{PHs\ and\ DHs} + \dot{W}_{net})/(1+i)^n\right)} \tag{27}$$

where the N is the lifetime of system (25 years), $\dot{Q}_{PHs\ and\ DHs}$ is the heat supply for the PH and DH, $\dot{W}_{net}$ is the output power.

3.4. NSGA II

The NSGA-II method stands out as a computationally efficient approach for discovering optimal solutions to multi-objective problems. Its key differentiating characteristics include a swift, non-dominated sorting procedure, an elitist strategy, and a parameter-free crowding distance assignment technique (Oyekale et al., 2020). The optimization process culminates by satisfying a predetermined repetition condition and subsequently yields the Pareto front. This achievement is made possible through the implementation of an elitist strategy, which preserves a significant portion of the newly generated population at each cycle. In our current study, we have selected LCOE and CO_2 emissions as the primary objective functions for optimization. The aim of this optimization is to minimize both LCOE and CO_2 emissions. Drawing from prior research, six key parameters were identified to serve as decision variables. The number of solar collectors N, the extraction percentage α, the inlet temperature of the evaporator T_7, the inlet temperature of the second turbine T_{16}, the pinch temperature of the evaporator, and the mass flow rate of the solar collector $\dot{m}_7$.

3.5. TOPSIS

The final Pareto frontier solution is chosen using the TOPSIS approach, which Hwang and Yoon developed in 1981 (Hwang and Yoon, 1981). The optimal alternative has both the shortest distance from the ideal solution, and the most significant distance from the perfect negative solution. TOPSIS seeks to rank the other options by calculating their distances from the perfect solution and the negative ideal solution (Chen, 2021). The following formula represents the bi-objective function matrix:

$$|A_{11} B_{12} A_{21} B_{22} \vdots \vdots A_{m1} B_{m2}| \tag{28}$$

After normalized the matrix can be expressed as:

$$|A'_{11} B'_{12} A'_{21} B'_{22} \vdots \vdots A'_{m1} B'_{m2}| \tag{29}$$

The most crucial part of TOPSIS is the weight coefficients. In our present work, A represents LCOE, and B represents CO_2 emission, the weight coefficients of LCOE and CO_2 emission are 0.6 and 0.4, respectively.

$$|A'_{11} B'_{12} A'_{21} B'_{22} \vdots \vdots A'_{m1} B'_{m2}||0.6\ 0\ 0\ 0.4| = |f_{11} f_{12} f_{21} f_{22} \vdots \vdots f_{m1} f_{m2}| \tag{30}$$

Each Pareto front solution's separation from the ideal solution is expressed as follows:

$$d_{i+} = \sqrt{\sum_{j=1}^{m} \left(f_{ij} - f_{ij}^{ideal}\right)^2} \tag{31}$$

Similarly, the distance between each Pareto front solution and nonideal solution is:

$$d_{i-} = \sqrt{\sum_{j=1}^{m} \left(f_{ij} - f_{ij}^{nonideal}\right)^2} \tag{32}$$

$$d = \frac{d_{i+}}{(d_{i+} + d_{i-})} \tag{33}$$

The ideal option is the one with the highest ranking (Wang et al., 2021).

4. Model validation

The authors validated the system's essential components to guarantee the accuracy of the analysis results. Since the suggested system has not been studied previously, the subsystem individual validation was based on the published data by Yu (Yu et al., 2021) and Yang (Yang et al., 2019), separately. The results of the current investigation and the references for the ORC cycle are compared in Table 4. The outcomes are consistent when compared to the literature. A different summer day was chosen for this analysis and led to a distinct DNI value and can be considered a minor inaccuracy.

Table 4
Comparison with Yu et al. and Yang et al. with the working fluid toluene for basic ORC cycle.

Model	$T_{hot}(^\circ C)$	$T_{cold}(^\circ C)$	$P_{eva}(bar)$	$T_{tur}^{inlet}(^\circ C)$	η_{orc} (%)	η_{sys} (%)
Yang et al. (Yang et al., 2019)	375	71.7	37.12	311.5	22.2	14.9
Current work	375	71.7	37.12	311.5	22.2	14.82
Yu et al. (Yu et al., 2021)	368	57.6	37.12	313.3	24.3	17.4
Current work	368	57.6	37.12	313.3	24.3	16.3

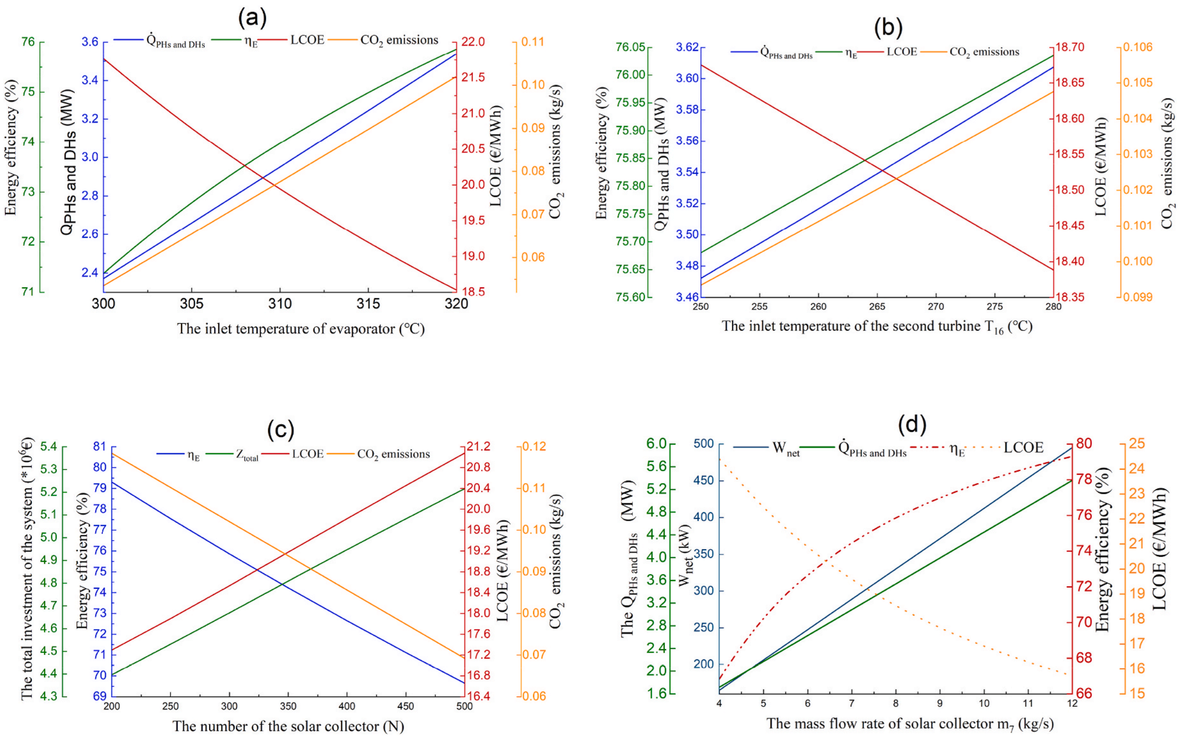

Fig. 2. The effect of T_7 (a), T_{16} (b) on total heat supply, energy efficiency, LCOE, and CO_2 emissions of the hybrid system ($N = 300, \dot{m}_7 = 8kg/s, T_{10} = 245°C$); the effect of N (c) on energy efficiency, total investment, LCOH, and CO_2 emissions, and effect of $\dot{m}_7$ (d) on the power output $\dot{W}_{net}$, $\dot{Q}_{PHs\ and\ DHs}$, η_E, and payback time ($T_7 = 320°C, \alpha = 0.6, T_{10} = 245°C$).

5. Results and discussion

5.1. Parametric analysis

The performance of the hybrid system (Fig. 2 a) represents the four parameters of the system: the total heat supply ($\dot{Q}_{PHs\ and\ DHs}$), energy efficiency η_E, LCOE, and CO_2 emissions (which varies depending on the inlet temperature of the evaporator). The $\dot{Q}_{PHs\ and\ DHs}$, and η_E increase as the temperature increases. Meanwhile, the LCOE decreases when the temperature increases. The reason is that the heat transfer to the ORC increases when the temperature increases. As a result, the output power and energy boost increase at the same time, so the energy efficiency of the system rises.

The definition of LCOE is related to the system output energy. When the output energy increases, the LCOE is reduced. According to Fig. 2a, the CO_2 emissions also increase along with T_7. Due to the environment-friendly aspect, low CO_2 emissions and LCOE are expected. Despite that, the two parameters conflict with each other. For the hybrid system, when T_7 is varied from 300 to 320 °C, the η_E ranges from 71.37% to 75.86%, respectively. To this extent, T_7 is the main feature affecting the system.

The influence of the second turbine T_{16} was investigated in Fig. 2b. The overall change trend of the four parameters is similar to Fig. 2a. The CO_2 emissions increase with the T_{16} increase. When T_{16} is equal to 280 °C, the CO_2 emissions is 0.1048 kg/s. CO_2 emissions are strongly dependent on the quality of MSW. Due to the increasing temperature, the mass of MSW increases, therefore, the CO_2 emissions also increase. The η_E also increase with the T_{16} increase (300–320 °C), the variation range is from 75.68% to 76.04%, respectively. For the other two parameters, LCOE and $\dot{Q}_{PHs\ and\ DHs}$, with the increase of T_{16}, the output energy increases, and the LCOE decreases. The energy efficiency raised along with T_{16}. According to Table 2, the output power of the second turbine increases as T_{16} increases, it means the $\dot{Q}_{DH2}$ increases, as a result, the η_E increases. Then, T_{16} is also a primary factor influencing the system performance.

The number of solar collectors also influences the system's performance. The outlet temperature of the HT is set to 280 °C. When the number of collectors increases, more WF is heated through the collector, which means the WI plant does not need to provide additional heat to warm the WF. The higher the number of solar collectors, the lower the energy that the WI plant must supply. However, the number of collectors (N) cannot increase infinitely. The critical point is that the mass flow of the WF heated by the collector is just enough for the ORC cycle (at this point the WI unit does not need to supply heat for the WF coming from HT). If it continues to grow, the output of the whole system is stable. The only part changing is the excess WF which will be stored in the HT, increasing the capacity of the HT and the consumption.

The energy efficiency, total investment, LCOE, and CO_2 emissions influenced by the number of solar collectors are shown in Fig. 2c. The LCOE grows along with the collector number. In this work, the investment in solar collectors accounted approximately for 47% of the total initial investment. With the increase of the solar collector's capacity, the total initial investment increased, due to the increase of the LCOE. The energy efficiency and CO_2 emissions decrease based on the increase of N. Since increasing N means decreasing WI, the CO_2 emissions decrease as well. The efficiency of SC is lower than the WI, in this way, the η_E also decreases with the increase of N. The lower the LCOE, the higher CO_2 emissions.

The results presented in Fig. 2d are related to the power output $\dot{W}_{net}$, $\dot{Q}_{PHs\ and\ DHs}$, η_E, and LCOE of the proposed system. $\dot{m}_7$ increases in power output, so the amount of power produced by the hybrid system is higher. The heat absorbed by the ORC is related to $\dot{m}_7$ (along with the increase of $\dot{m}_7$) because the heat absorbed by ORC increases. Therefore, the power output is higher. The $\dot{Q}_{PHs\ and\ DHs}$ changes proportionally with $\dot{W}_{net}$. The η_E increases with the increase of $\dot{m}_7$. The variability of η_E is between 66.83% and 79.3%. It is noticed that LCOE decrease as $\dot{m}_7$ increases, when $\dot{m}_7$ is equal to 12 kg/s, LCOE is 15.72 €/MWh. The influence of the percentage of the first turbine α is shown in Fig. 3.

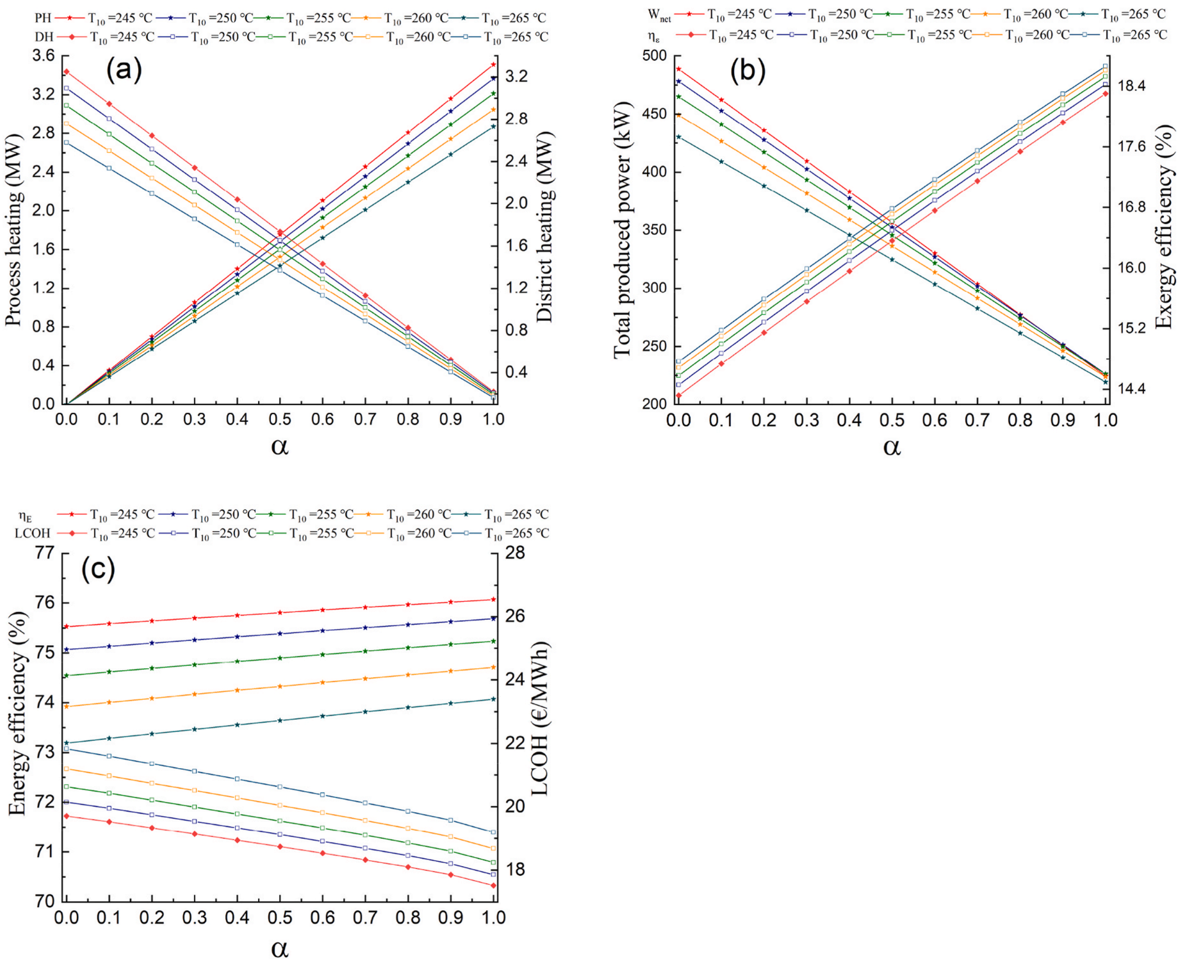

Fig. 3. The influence of various rates of α on PH and DH supply (a), total produced power and exergy efficiency (b), and energy efficiency and LCOE ($N = 300, \dot{m}_7 = 8kg/s$).

The inlet temperature of the first turbine T_{10} effectively influences the properties of the system. In Fig. 3a, α varies from 0 to 1. From the schematic of the system, the PH supply comes from the extraction of the first turbine. When $\alpha = 0$, it means there is no energy extraction from the first turbine for PH supply, otherwise, it has PH supply. Thus, if the extraction factor α rises, the PH supply also increases. Moreover, the DH supply is composed of two parts. The first DH (DH1) is connected to the second turbine, and the second DH (DH2) is connected to the flue gas. When α rises, the DH2 is still constant, meanwhile, the WF going through the second turbine is decreased. According to Fig. 3a, DH supply decreases as α increases, this happens because part of the energy extracted from the first turbine is provided to the PH, so the DH supply is the lowest when $\alpha = 1$.

It also should be noticed that, as T_{10} increases, the DH and PH supply all decrease. In case all the WF goes through the first turbine ($\alpha = 1$), 3.51 MW more PH might be supplied if T_{10} is equal to 245 °C. This can be decreased to 2.87 MW if T_{10} is equal to 265 °C. The output powers $\dot{W}_{net}$ consists of two parts, which come from the first turbine and second turbine. For the case $\alpha = 0$, all the energy that the ORC cycle receives from the solar-WI plant is to generate power. Otherwise, part of the WF is extracted to create heat for PH and DH supply. The more WF is extracted, the less power is generated. That is the reason the $\dot{W}_{net}$ is decreased.

Fig. 3b shows the variation of the total produced power ($\dot{W}_{net}$), and exergy efficiency (η_ε) for different values of α. As α rises, η_ε rises as well, furthermore, η_ε also rises when T_{10} increases. When $T_{10} = 265°C$ and $\alpha = 1$, the η_ε reaches the maximum value. However, under the same α, there is a small difference in η_ε. Opposite to η_ε, the amount of produced power decreases. The improvement of heat supply is based on the premise of reducing the output power. Without PH supply ($\alpha = 0$), the maximum of $\dot{W}_{net}$ is 488.7 kW is obtained ($T_{10} = 245°C$).

Fig. 3c shows the energy efficiency and LCOE for different α. According to the figure, the energy efficiency is maximized when $\alpha = 1$. At this point, the energy efficiency is 76.07% as T_{10} is equal to 245 °C. Based on equations (12) and (27), if the energy efficiency goes up, the LCOE must go down. In addition, it is seen that the value of α dramatically impacts the overall system performance. A possible reason for the increase in efficiency is that when the extraction percentage rises, more WF flows through the heat exchanger to generate more heat for supplying the PH and DH. According to the observations, the best performance of energy efficiency and LCOE is when $T_7 = 245°C, \alpha = 1$.

5.2. Environment analysis

One of the goals of this study is to discuss the environmental impacts of the hybrid system. Solar energy is environment-friendly since it does not emit carbon dioxide during operation. The quantification of CO_2 equivalent emissions in a WI process can be mathematically determined by the following equation (Sadi and Arabkoohsar, 2019b):

$$E_{CO_2} = GWP_\lambda E_\lambda \tag{34}$$

$$E_\lambda = \xi M \mu_\lambda \tag{35}$$

where GWP_λ is the global warming potential of a specific greenhouse gas

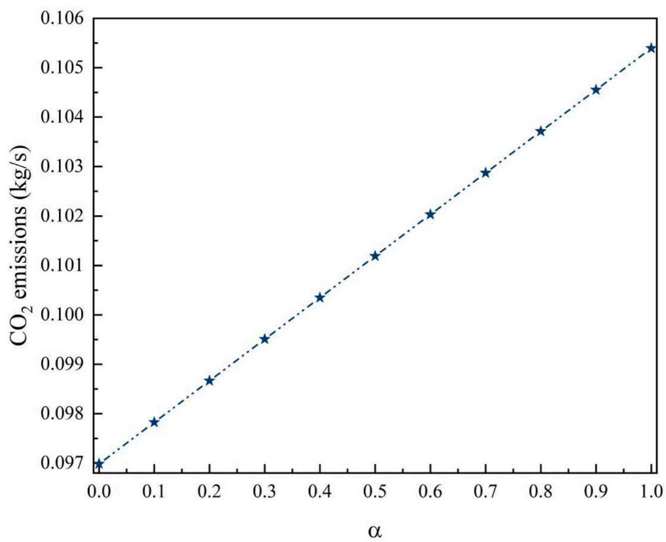

Fig. 4. The carbon dioxide emission varies with the α ($N = 300, \dot{m}_7 = 8kg/s$, $T_{10} = 245°C$).

is assessed as the amount of CO_2 pollution emitted per ton of the gas in question. E_λ represents the emissions of various types of greenhouse gasses, ξ denotes the volume of exhaust gasses, M represents the mass of the waste material, μ_λ signifies the concentration of the emitted gas. Taking into account the advice in (Nami et al., 2020), the amount of CO_2 production is entirely by the WI plant during the working process, which is 415 kg per ton. However, the commonly used garbage disposal method is landfilling. An average municipal solid waste landfill produces 840 kg of CO_2 per ton. Therefore, it can reduce 425 kg of CO_2 emitted per ton as a heat resource.

The WI unit is a robust secondary energy source that guarantees the twenty-four uninterrupted output of electricity and heat. The capacity of the WI plant varies depending on solar energy. Fig. 4 demonstrates how α influences CO_2 production. When $\alpha = 1$, CO_2 emission achieves the maximum value of 0.1054 kg/s. However, comparing Figs. 3c and 4, the energy efficiency increases with the rise of α. At the same time, CO_2 production also increases. Fig. 3c shows that the LCOE reaches the ideal value when $\alpha = 1$. Since a lower LCOE and a lower CO_2 emission are the main goals of this work, the choice between the two variables is considered.

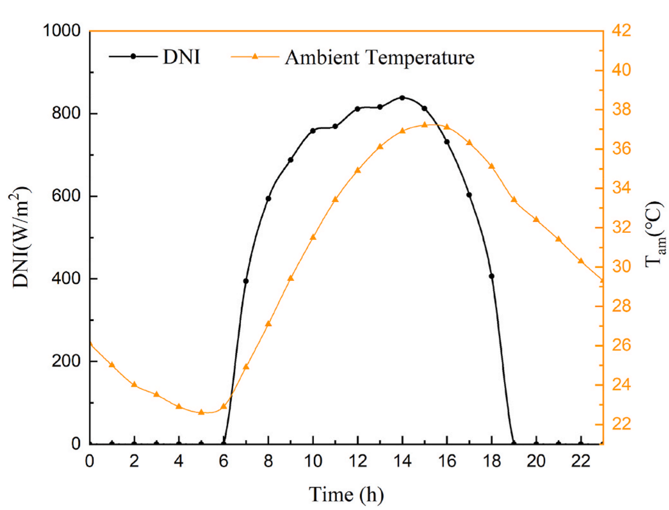

Fig. 5. DNI distribution and ambient temperature for the specific day.

Table 5
The input parameters of NSGA-II.

Parameters	Value/range
Generation size	120
Crossover fraction	0.8
Selection process	Tournament
Migration fraction	0.2
Maximum generation	40
The number of collectors (N)	260–400
The value of α	0.0–1.0
The inlet temperature of the evaporator T_7 (k)	570–590
The inlet temperature of the second turbine T_{16} (k)	520–535
pinch temperature of the evaporator (k)	5–15
Mass flow rate of SC cycle $\dot{m}_7$ (kg/s)	3–12

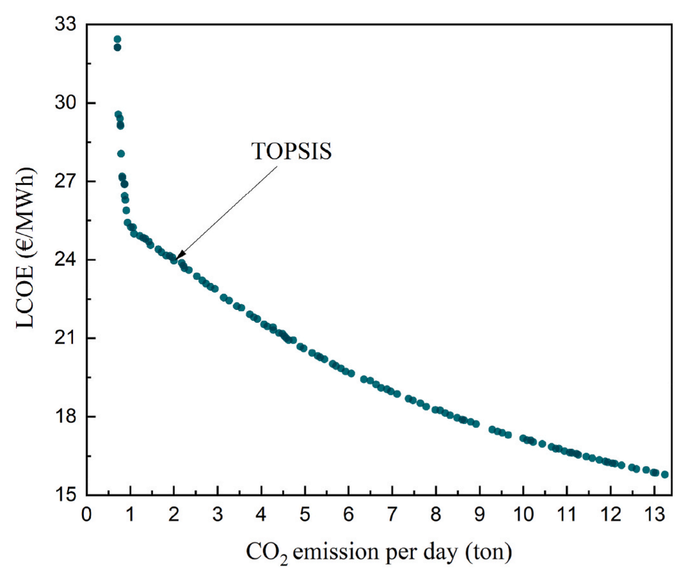

Fig. 6. The Pareto boundary for optimal points of the hybrid system.

5.3. *Optimization results*

Our present work used the LCOE and CO_2 emissions as the two target functions for the hybrid system optimization. For making the optimization realistic, as solar energy is an effective parameter and fluctuates sharply, there must be a case study. Yinchuan, situated in the north-western region of China, boasts an abundance of sunshine, making it an ideal locale for harnessing solar energy. Here it is assumed that the city of Yinchuan is where the proposed plant is to be established. Solar irradiation during the whole year 2020 was recorded in Yinchuan and has been used for the simulations and optimizations here. It is important to note that this type of solar collector as a concentrating solution can only use the beam component of solar irradiation. The DNI and ambient temperature of the case study for a specific day are given in Fig. 5, derived from Meteonorm software. The simulation process can be described as follows: during daytime the WF through the solar collector is heated. In cases where the DNI is not adequate, the WI unit is employed to ensure that the evaporator's inlet temperature remains at an appropriate level. After undergoing heat exchange in the evaporator, the WF within the ORC system is utilized to generate both power and heat supply simultaneously.

To analyze the whole system, several assumptions were made, such as: steady state during the system operations, constant DNI distribution and ambient temperature per hour, negligible piping pressure drop and heat loss from heat exchangers. The parameter in NSGA-II is given in Table 5. The Pareto boundary is shown in Fig. 6. From Fig. 6, it is noticed that the two objectives (LCOE and CO_2 emission) conflict with each other. Each point that the Pareto frontier solution introduces can be

Table 6
The parameters of the optimization point chosen by TOPSIS.

Parameters	Value (hybrid system)	Value ($\alpha = 0$)
CO_2 emission (ton per day)	1.9995	2.1977
Levelized cost of energy LCOE (€/MWh)	23.96	28.67
The number of solar collectors N	313	313
percentage of steam extraction α	0.92	0
The inlet temperature of evaporator T_7 (k)	579.3	579.3
The inlet temperature of the second turbine T_{16} (k)	526	526
The pinch point temperature of the evaporator ΔT_{eva} (k)	11.78	11.78
The mass flow rate of solar collector m_7 (kg/s)	5.38	5.38
The power output $\dot{W}_{net}$ (kW)	124.98	245.73
The PH supply of the system $\dot{Q}_{PHs}$ (kW)	1647.21	0
The DH supply of the system $\dot{Q}_{DHs}$ (kW)	167.53	1544.14
The total energy output ($\dot{W}_{net} + \dot{Q}_{PHs} + \dot{Q}_{DHs}$) (kW)	1939.72	1789.87
The energy efficiency of the system $\dot{\eta}_E$ (%)	65.46	58.90
The exergy efficiency of the system $\dot{\eta}_\varepsilon$ (%)	16.33	11.81
The total investment Z_{total} (*10^6€)	3.03	3.34
Payback time (years)	2.82	4.05

chosen as an ideal point. The decision-maker can select their top choice based on the importance of the objective function. In our present work, the TOPSIS method was used for the decision making: the ideal point was marked in Fig. 6, the parameters are listed in Table 6. The LCOE is 23.96 €/MWh, which is more realistic; and the CO_2 emission is 1.9995 tons per day, which is equal to 729.8 tons per year. Compared to landfilling, the CO_2 emissions are reduced by 747.4 tons per year.

5.4. System performance under optimized conditions

Based on the ideal point chosen by TOPSIS, the authors analyzed the performance of the Fresnel lens thermal collector-WI hybrid system. The original intention of designing the system is to increase the PHs and DHs supply. When the percentage of steam extraction from the first turbine reaches 0.92, the PHs supply goes up to 1647.21 kW, and the DHs is 167.53 kW. Under the same condition, without the PHs supply extraction, the DHs supply is 1544.14 kW. The total energy output is also given in Table 6. The energy amount of the hybrid system is higher which results in a high energy efficiency of 65.46%. The LCOE with PHs supply and without PHs supply is 23.96 €/MWh and 28.67 €/MWh, respectively.

The exergy destruction percentage of each component is shown in Fig. 7. Most of the exergy destruction comes from SC and WI. The exergy destruction of the two components reaches 68.33% for the SC and 19.58% for the WI. The exergy efficiency of the hybrid system is 16.33% which has a 4.52% improvement after the modified system design. The economic performance of the hybrid system is also superior, the total investment was reduced by 0.31 million, and the payback time was reduced from 4.05 to 2.82 years. Hassan et al. (2022) have introduced a hybrid system and presented a case study focused on Alexandria city in Egypt. Their findings revealed an exergy efficiency of 11.1% and a payback time of 8.45 years. In comparison to their system, the one presented in the current work demonstrates an exceptionally dominant performance.

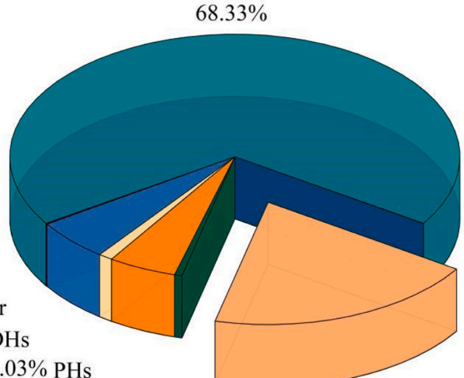

Fig. 7. The exergy destruction percentage of each component.

6. Conclusions

This study proposed a hybrid solar-waste system for multi-generation. There are different facts that make this system innovative. The first fact was the use of a new generation of Fresnel lens medium-temperature solar collectors which has not been studied in scientific literature. The second fact is the way the system is used for multi-generation and more specifically PH at different temperature levels to tackle the challenges associated with the decarbonization of the industry which is currently very expensive to do so. The article presents a thorough energy, exergy, economic, and environmental performance analysis of the system and a multi-objective optimization to not only bring out the most optimal design of the proposed cycle, but also get a profound understanding of the system strengths, drawbacks, sensitivities to different performance parameters, etc. NSGA II is used to optimize the objective functions (LCOE and CO_2 emissions), Pareto front was obtained under six decision variables; and the TOPSIS decision-maker method was used to choose the ideal solution. For making the study of practical value, a case study is considered for that, i.e. Yinchuan, China. As PH is one of the important outputs of the developed hybrid solution, a base case design of the plant is also considered in which PH is not considered and thus the cycle acts as a CHP (only supplying low-grade heat for the DH systems and power for the grid). The same sorts of analysis and optimizations on this base case is also conducted and then the results are compared to that of the main multi-generation case in terms of energy and exergy efficiencies, total investment, payback time, total supply, and CO_2 emissions. Following, the main conclusions and findings of this analysis are presented.

- The solar collector type could perform very effectively in lowering the cost of solar heat supply at temperature grades suitable for power generation. Here as the medium-temperature level is achievable, using an ORC is a must.
- PH supply could give the system very great economic value and enhance its cost-effectiveness, but more importantly, it is of great practical value as this way the system could tackle one of the challenges of the green transition, which is green industrial processes.

- $\dot{Q}_{PHs\ and\ DHs}$, η_E, and CO_2 emissions increase as the inlet temperature of the evaporator T_7 or the inlet temperature of the second turbine T_{16} increases, but the LCOE decreases.
- LCOE and total investment costs have a direct relation to the number of solar collectors (share of the solar energy in the overall supply), but a reverse relation to η_E, and CO_2 emissions.
- $\dot{Q}_{PHs\ and\ DHs}$, η_E, and $\dot{W}_{net}$ rise as the mass flow rate m_4 increase, as a result the techno-economic performance gets better, lowering the LCOE.
- The inlet temperature of the first turbine T_{10} and the percentage of steam extraction α turn out to be two key decision parameters of the system performance. When $T_{10} = 245^{\circ}C$, the economic performance is better, and there is more steam extraction and more PH supply.
- The LCOE and CO_2 emissions per day were chosen to be the optimized objective functions. TOPSIS provides the ideal point: the LCOE is 23.96 €/MWh, and the CO_2 emission is 1.9995 tons per day.
- Under the ideal point condition, the energy and exergy efficiencies are 65.46% and 16.33%, respectively. The PH supply is 1647.21 kW, payback time is 2.82 years, power output is 124.98 kW, and DH supply is 167.53 kW.
- Among the system components, the collectors and WI are majorly responsible for the exergy destructions. The exergy destruction rate of the Fresnel lens collectors is around 68.33%.

This approach emphasizes the integration of solar energy with WI. Future research endeavors may explore the synergies between solar energy and other sustainable sources, such as wind energy and geothermal energy. Additionally, it's worth noting that our current study did not consider variations in WF, which is a significant factor that can impact the system's performance.

Author contributions statement

Lina Wang: Conceptualization, Methodology, Software, Formal analysis, Writing - Original Draft; Mavd P. R. Teles: Supervision, Reviewing and Editing; Haoshui Yu: Conceptualization, Reviewing and Editing; Brenda V. F. Silva: Idea maturation, Reviewing; Ahmad Arabkoohsar: Conceptualization, Methodology, Supervision, Review and Editing.

Declaration of competing interest

None of the authors see any conflicts of interest.

Data availability

Data will be made available on request.

Acknowledgement

A scholarship financially supports this article from China Scholarships Council under Grant 202008210357.

References

Aboelwafa, O., Fateen, S.E.K., Soliman, A., Ismail, I.M., 2018. A review on solar Rankine cycles: working fluids, applications, and cycle modifications. Renew. Sustain. Energy Rev. 82, 868–885. https://doi.org/10.1016/J.RSER.2017.09.097.

Aghaziarati, Z., Aghdam, A.H., 2021. Thermoeconomic analysis of a novel combined cooling, heating and power system based on solar organic Rankine cycle and cascade refrigeration cycle. Renew. Energy 164, 1267–1283. https://doi.org/10.1016/j.renene.2020.10.106.

Alirahmi, S.M., Mousavi, S.F., Ahmadi, P., Arabkoohsar, A., 2021a. Soft computing analysis of a compressed air energy storage and SOFC system via different artificial neural network architecture and tri-objective grey wolf optimization. Energy 236, 121412. https://doi.org/10.1016/j.energy.2021.121412.

Alirahmi, S.M., Assareh, E., Chitsaz, A., Ghazanfari Holagh, S., Jalilinasrabady, S., 2021b. Electrolyzer-fuel cell combination for grid peak load management in a geothermal power plant: power to hydrogen and hydrogen to power conversion. Int. J. Hydrogen Energy 46, 25650–25665. https://doi.org/10.1016/j.ijhydene.2021.05.082.

Alirahmi, S.M., Behzadi, A., Ahmadi, P., Sadrizadeh, S., 2023. An innovative four-objective dragonfly-inspired optimization algorithm for an efficient, green, and cost-effective waste heat recovery from SOFC. Energy 263, 125607. https://doi.org/10.1016/j.energy.2022.125607.

Allouhi, A., Saadani, R., Buker, M.S., Kousksou, T., Jamil, A., Rahmoune, M., 2019. Energetic, economic and environmental (3E) analyses and LCOE estimation of three technologies of PV grid-connected systems under different climates. Sol. Energy 178, 25–36. https://doi.org/10.1016/j.solener.2018.11.060.

Amen, R., Hameed, J., Albashar, G., Kamran, H.W., Hassan Shah, M.U., Zaman, M.K.U., et al., 2021. Modelling the higher heating value of municipal solid waste for assessment of waste-to-energy potential: a sustainable case study. J. Clean. Prod. 287. https://doi.org/10.1016/j.jclepro.2020.125575.

Arabkoohsar, A., Nami, H., 2019. Thermodynamic and economic analyses of a hybrid waste-driven CHP–ORC plant with exhaust heat recovery. Energy Convers. Manag. 187, 512–522. https://doi.org/10.1016/j.enconman.2019.03.027.

Behzadi, A., Arabkoohsar, A., Perić, V.S., 2021. Innovative hybrid solar-waste designs for cogeneration of heat and power, an effort for achieving maximum efficiency and renewable integration. Appl. Therm. Eng. 190 https://doi.org/10.1016/j.applthermaleng.2021.116824.

Bellos, E., Tzivanidis, C., 2018. Investigation of a hybrid ORC driven by waste heat and solar energy. Energy Convers. Manag. 156, 427–439. https://doi.org/10.1016/j.enconman.2017.11.058.

Braimakis, K., Charalampidis, A., Karellas, S., 2021. Techno-economic assessment of a small-scale biomass ORC-CHP for district heating. Energy Convers. Manag. 247, 114705 https://doi.org/10.1016/j.enconman.2021.114705.

Chen, P., 2021. Effects of the entropy weight on TOPSIS. Expert Syst. Appl. 168, 114186 https://doi.org/10.1016/j.eswa.2020.114186.

Chen, H., Zhao, L., Cong, H., Li, X., 2022. Synthesis of waste heat recovery using solar organic Rankine cycle in the separation of benzene/toluene/p-xylene process. Energy 255, 124443. https://doi.org/10.1016/j.energy.2022.124443.

Coskun, C., Oktay, Z., Ilten, N., 2009. A new approach for simplifying the calculation of flue gas specific heat and specific exergy value depending on fuel composition. Energy 34, 1898–1902. https://doi.org/10.1016/j.energy.2009.07.040.

Crespo, A., Barreneche, C., Ibarra, M., Platzer, W., 2019. Latent thermal energy storage for solar process heat applications at medium-high temperatures – a review. Sol. Energy 192, 3–34. https://doi.org/10.1016/j.solener.2018.06.101.

Desai, N.B., Pranov, H., Haglind, F., 2021. Techno-economic analysis of a foil-based solar collector driven electricity and fresh water generation system. Renew. Energy 165, 642–656. https://doi.org/10.1016/j.renene.2020.11.043.

Desai, N.B., Mondejar, M.E., Haglind, F., 2022. Techno-economic analysis of two-tank and packed-bed rock thermal energy storages for foil-based concentrating solar collector driven cogeneration plants. Renew. Energy 186, 814–830. https://doi.org/10.1016/j.renene.2022.01.043.

Escamilla-García, P.E., Camarillo-López, R.H., Carrasco-Hernández, R., Fernández-Rodríguez, E., Legal-Hernández, J.M., 2020. Technical and economic analysis of energy generation from waste incineration in Mexico. Energy Strategy Rev. 31 https://doi.org/10.1016/j.esr.2020.100542.

Farjana, S.H., Huda, N., Mahmud, M.A.P., Saidur, R., 2018. Solar industrial process heating systems in operation – current SHIP plants and future prospects in Australia. Renew. Sustain. Energy Rev. 91, 409–419. https://doi.org/10.1016/j.rser.2018.03.105.

Fixed and variable costs for the operation and maintenance of new power plants in the United States as of 2021, by technology type. Stat, 2021. https://www.statista.com/statistics/519144/power-plant-operation-and-maintenance-costs-in-the-us-by-technology/.

Gao, D., Kwan, T.H., Dabwan, Y.N., Hu, M., Hao, Y., Zhang, T., et al., 2022. Seasonal-regulatable energy systems design and optimization for solar energy year-round utilization. Appl. Energy 322, 119500. https://doi.org/10.1016/j.apenergy.2022.119500.

Gomaa, M.R., Mustafa, R.J., Al-Dhaifallah, M., Rezk, H., 2020. A low-grade heat Organic Rankine Cycle driven by hybrid solar collectors and a waste heat recovery system. Energy Rep. 6, 3425–3445. https://doi.org/10.1016/j.egyr.2020.12.011.

Gowrisankaran, G., Reynolds, S.S., Samano, M., 2016. Intermittency and the Value of Renewable Energy 124, 1187–1234. https://doi.org/10.1086/686733. Https://DoiOrg/101086/686733.

Hassan, A.A., Elwardany, A.E., Ookawara, S., Sekiguchi, H., Hassan, H., 2022. Energy, exergy, economic and environmental (4E) assessment of hybrid solar system powering adsorption-parallel/series ORC multigeneration system. Process Saf. Environ. Protect. 164, 761–780. https://doi.org/10.1016/j.psep.2022.06.024.

He, J., Lin, B., 2019. Assessment of waste incineration power with considerations of subsidies and emissions in China. Energy Pol. 126, 190–199. https://doi.org/10.1016/j.enpol.2018.11.025.

Hwang, C.-L., Yoon, kwangsun, 1981. Multiple Attribute Decision Making: Methods and Applications. Springer Berlin Heidelberg, New York.

Jack, T.A., Oko, C.O.C., 2017. Https://DoiOrg/101080/0143075020171305447 Exergy and exergoeconomic analysis of a municipal waste-to-energy steam reheat power plant for Port Harcourt city 39. https://doi.org/10.1080/01430750.2017.1305447, 352–9.

Jafary, S., Khalilarya, S., Shawabkeh, A., Wae-hayee, M., Hashemian, M., 2021. A complete energetic and exergetic analysis of a solar powered trigeneration system with two novel organic Rankine cycle (ORC) configurations. J. Clean. Prod. 281, 124552 https://doi.org/10.1016/j.jclepro.2020.124552.

Jie Ling, J.L., Go, E.S., Park, Y.K., Lee, S.H., 2022. Recent advances of hybrid solar - biomass thermo-chemical conversion systems. Chemosphere 290. https://doi.org/10.1016/J.CHEMOSPHERE.2021.133245.

Jinshah, B.S., Balasubramanian, K.R., Ravikumar, K., Divakar, S., 2023. A dual-mode novel Parabolic Trough Collector for process heating applications in small scale industries—thermo-hydraulic and performance investigation. Appl. Therm. Eng. 218, 119287 https://doi.org/10.1016/j.applthermaleng.2022.119287.

Kalbasi, R., Samali, B., Afrand, M., 2023. Taking benefits of using PCMs in buildings to meet energy efficiency criteria in net zero by 2050. Chemosphere 311, 137100. https://doi.org/10.1016/J.CHEMOSPHERE.2022.137100.

Kumar, L., Hasanuzzaman, M., Rahim, N.A., 2019. Global advancement of solar thermal energy technologies for industrial process heat and its future prospects: a review. Energy Convers. Manag. 195, 885–908. https://doi.org/10.1016/j.enconman.2019.05.081.

Li, Y.R., Wang, J.N., Du, M.T., 2012. Influence of coupled pinch point temperature difference and evaporation temperature on performance of organic Rankine cycle. Energy 42, 503–509. https://doi.org/10.1016/j.energy.2012.03.018.

Liu, Y., Yan, G., Albdeiri, M.S., Singh Chauhan, B., Salah, B., Saleem, W., et al., 2023. Techno-economic analysis and optimization of near-zero energy and emission neighborhoods using biomass waste. Chemosphere, 138978. https://doi.org/10.1016/J.CHEMOSPHERE.2023.138978.

Mehrpooya, M., Ghorbani, B., Khalili, M., 2021. A new developed integrated process configuration for production of hydrogen chloride using geothermal and wind energy resources. Sustain. Energy Technol. Assessments 45, 101173. https://doi.org/10.1016/j.seta.2021.101173.

Meriño Stand, L., Valencia Ochoa, G., Duarte Forero, J., 2021. Energy and exergy assessment of a combined supercritical Brayton cycle-orc hybrid system using solar radiation and coconut shell biomass as energy source. Renew. Energy 175, 119–142. https://doi.org/10.1016/J.RENENE.2021.04.118.

Morais, PH. da S., Lodi, A., Aoki, A.C., Modesto, M., 2020. Energy, exergetic and economic analyses of a combined solar-biomass-ORC cooling cogeneration systems for a Brazilian small plant. Renew. Energy 157, 1131–1147. https://doi.org/10.1016/j.renene.2020.04.147.

Nami, H., Arabkoohsar, A., Anvari-Moghaddam, A., 2019. Thermodynamic and sustainability analysis of a municipal waste-driven combined cooling, heating and power (CCHP) plant. Energy Convers. Manag. 201, 112158 https://doi.org/10.1016/j.enconman.2019.112158.

Nami, H., Anvari-Moghaddam, A., Arabkoohsar, A., Razmi, A.R., 2020. 4E analyses of a hybrid waste-driven CHP–ORC plant with flue gas condensation. Sustain. Times 12, 1–21. https://doi.org/10.3390/su12229449.

Naquash, A., Qyyum, M.A., Chaniago, Y.D., Riaz, A., Yehia, F., Lim, H., et al., 2023. Separation and purification of syngas-derived hydrogen: a comparative evaluation of membrane- and cryogenic-assisted approaches. Chemosphere 313. https://doi.org/10.1016/J.CHEMOSPHERE.2022.137420.

Newell, R.G., Raimi, D., Aldana, G., 2019. Global energy outlook 2019: the next generation of energy. Resour Futur 46.

Olabi, A.G., Elsaid, K., Sayed, E.T., Mahmoud, M.S., Wilberforce, T., Hassiba, R.J., et al., 2021. Application of nanofluids for enhanced waste heat recovery: a review. Nano Energy 84, 105871. https://doi.org/10.1016/j.nanoen.2021.105871.

Ortiz, C., Tejada, C., Chacartegui, R., Bravo, R., Carro, A., Valverde, J.M., et al., 2021. Solar combined cycle with high-temperature thermochemical energy storage. Energy Convers. Manag. 241, 114274 https://doi.org/10.1016/J.ENCONMAN.2021.114274.

Oyekale, J., Petrollese, M., Cau, G., 2020. Multi-objective thermo-economic optimization of biomass retrofit for an existing solar organic Rankine cycle power plant based on NSGA-II. Energy Rep. 6, 136–145. https://doi.org/10.1016/j.egyr.2019.10.032.

Petrollese, M., Cocco, D., 2019. Robust optimization for the preliminary design of solar organic Rankine cycle (ORC) systems. Energy Convers. Manag. 184, 338–349. https://doi.org/10.1016/j.enconman.2019.01.060.

Pranov, H., Matschuk, M., Helic, A.P., 2019. Laminate Solar Concentrator, 081.

Ravi Kumar, K., Krishna Chaitanya, N.V.V., Sendhil Kumar, N., 2021. Solar thermal energy technologies and its applications for process heating and power generation – a review. J. Clean. Prod. 282. https://doi.org/10.1016/j.jclepro.2020.125296.

Rogelj, J., Huppmann, D., Krey, V., Riahi, K., Clarke, L., Gidden, M., et al., 2019. A new scenario logic for the Paris Agreement long-term temperature goal. Nature 573, 357–363. https://doi.org/10.1038/s41586-019-1541-4.

Sadi, M., Arabkoohsar, A., 2019a. Exergoeconomic analysis of a combined solar-waste driven power plant. Renew. Energy 141, 883–893. https://doi.org/10.1016/J.RENENE.2019.04.070.

Sadi, M., Arabkoohsar, A., 2019b. Modelling and analysis of a hybrid solar concentrating-waste incineration power plant. J. Clean. Prod. 216, 570–584. https://doi.org/10.1016/j.jclepro.2018.12.055.

Sadi, M., Arabkoohsar, A., Joshi, A.K., 2021. Techno-economic optimization and improvement of combined solar-powered cooling system for storage of agricultural products. Sustain. Energy Technol. Assessments 45, 101057. https://doi.org/10.1016/j.seta.2021.101057.

Sajid Khan, M., Huan, Q., Lin, J., Zheng, R., Gao, Z., Yan, M., 2022. Exergoeconomic analysis and optimization of an innovative municipal solid waste to energy plant integrated with solar thermal system. Energy Convers. Manag. 258, 115506 https://doi.org/10.1016/j.enconman.2022.115506.

Serda, Maciej, Becker, F.G., Cleary, M., Team, R.M., Holtermann, H., The, D., et al., 2022. REPowerEU and Fitfor55 science-based policy recommendations for achieving the energy efficiency first principle. Uniw Śląski 7, 343–354.

Shahsavari, A., Akbari, M., 2018. Potential of solar energy in developing countries for reducing energy-related emissions. Renew. Sustain. Energy Rev. 90, 275–291. https://doi.org/10.1016/j.rser.2018.03.065.

Song, J., Wang, Y., Wang, K., Wang, J., Markides, C.N., 2021. Combined supercritical CO2 (SCO2) cycle and organic Rankine cycle (ORC) system for hybrid solar and geothermal power generation: thermoeconomic assessment of various configurations. Renew. Energy 174, 1020–1035. https://doi.org/10.1016/J.RENENE.2021.04.124.

Teng, S., Wang, M., Xi, H., Wen, S., 2021. Energy, exergy, economic (3E) analysis, optimization and comparison of different ORC based CHP systems for waste heat recovery. Case Stud. Therm. Eng. 28, 101444 https://doi.org/10.1016/j.csite.2021.101444.

Wang, Z., Xia, X., Pan, H., Zuo, Q., Zhou, N., Xie, B., 2021. Fluid selection and advanced exergy analysis of dual-loop ORC using zeotropic mixture. Appl. Therm. Eng. 185, 116423 https://doi.org/10.1016/j.applthermaleng.2020.116423.

Yang, J., Li, J., Yang, Z., Duan, Y., 2019. Thermodynamic analysis and optimization of a solar organic Rankine cycle operating with stable output. Energy Convers. Manag. 187, 459–471. https://doi.org/10.1016/j.enconman.2019.03.021.

Yu, H., Helland, H., Yu, X., Gundersen, T., Sin, G., 2021. Optimal design and operation of an Organic Rankine Cycle (ORC) system driven by solar energy with sensible thermal energy storage. Energy Convers. Manag. 244, 114494 https://doi.org/10.1016/j.enconman.2021.114494.

Yu, D., Wan, X., Gu, B., 2023. Bi-objective optimization of biomass solid waste energy system with a solid oxide fuel cell. Chemosphere 323, 138182. https://doi.org/10.1016/J.CHEMOSPHERE.2023.138182.

Glossary

A: area, m^2
be: end collector loss
bsh: shadow collector loss
C: cash flow
cp: specific heat, J/(kg K)
DNI: direct normal solar irradiation, W/m^2
E: energy, J
h: enthalpy, J
$\dot{I}$: exergy destruction, W
Ja: sensible heat to latent heat ratio
K: element percentage
$\dot{m}$: mass flow rate, kg/s
N: number of solar collectors
$\dot{Q}$: heat flow, W
r: interest rate
s: entropy, J/kgK
T: temperature, °C
t: time, s
U: overall heat transfer coefficient, $W/m^2.K$
V: volume, m^3
Z: cost
$\dot{W}$: work, W
Y: net cash flow

Greek symbols

α: percentage of steam extraction
Δ: difference
λ: percentage of extra combustion air
ε: exergy flux
η: efficiency
ρ: density, kg/m^3

Subscripts and superscripts

0: standard conditions
ap: aperture
C: carbon
DH: district heating
e: electricity
E: energy
eva: evaporator
h: heat
H: hydrogen
HT: heat transfer
in: inlet
ins: installation
inv: investment
m: average
N: nitrogen
net: total output power
o: optical
O: oxygen
ope: operation
out: outlet
p: pump
PH: process heating
S: sulphur
SC: solar collector

sys: system
t: turbine
TES: thermal energy storage
WI: waste incinerator

Acronyms

PV: Photovoltaic
SC: Solar collector
MSW: municipal solid waste
CSP: concentrated solar power
PTC: parabolic trough collectors
IHE: Internal Heat Exchanger
OFOH: open feed-organic heater
IAM: incidence angle modifier
TES: thermal energy storage
LHV: lower heating value
HT: hot tank
LCOE: levelized cost of energy
ORC: organic Rankine cycle
NPV: net present value
WI: Waste incineration
MSPF: micro-structured polymer foil
LEC: levelized energy cost
EES: engineering equation solver
DH: district heating
HHV: higher heating values
PV: photovoltaic
ETC: evacuated tube collector
GHG: greenhouse emission
LCOC: levelized cost of cooling
LHV: lower calorific value
POF: Pareto-optimal front